Progress In Electromagnetics Research M, Vol. 75, 131–140, 2018

Polarizations of Crossed-Dipole Antenna Loaded with Different NFRP Elements

Son Xuat Ta*

Abstract—In this paper, the polarizations of single-feed crossed-dipole antennas loaded with different near-field resonant parasitic (NFRP) elements are investigated. The antennas are placed above a metallic reflector for a broadside radiation pattern. Meander line with an arrowhead-shaped ending is applied in all arms of the crossed-dipole and NFRP elements for the compactness. By adjusting the ending sizes of the NFRP element, the polarization of antenna can be right-hand circularly polarized (RHCP) — linearly polarized (LP) — left-hand circularly polarized (LHCP). For validation, two antennas with RHCP and LHCP performances are implemented and measured. The RHCP antenna yields a $|S_{11}| < -10$ dB bandwidth of 1.454–1.668 GHz (214 MHz) and a 3-dB axial ratio (AR) bandwidth of 1.525–1.585 GHz (60 MHz). The LHCP antenna yields a $|S_{11}| < -10$ dB bandwidth of 1.475–1.702 GHz (227 MHz) and a 3-dB AR bandwidth of 1.535–1.580 GHz (45 MHz). Moreover, both antennas yield a good broadside radiation with a gain of > 6.0 dBic and a radiation efficiency of $> 65\%$ across their operational bandwidth.

1. INTRODUCTION

Near field resonant parasitic (NFRP) antennas [1], which is a typical example of metamaterial (MTM) based antennas [2], have been widely developed for a variety of wireless communication systems due to their compact physical sizes in terms of operational wavelengths, multi-function, good impedance matching, good circularly polarized (CP) radiation, and high radiation efficiency (RE). An NFRP antenna is conventionally constructed from a single MTM unit cell, which is properly incorporated with an electrically small driven element to achieve a nearly complete impedance matching and high RE [3]. In order to achieve other features, such as multi-frequency [4], CP radiation [5–8], or directive radiation with no ground [9], the electrically small driven elements have to be incorporated with two or more NFRP elements properly. Therefore, the configurations of these antennas are complicated, and consequently, it is relatively difficult to implement the CP NFRP antennas for multiband operations or enhance their operational bandwidths. Recently, the crossed-dipole NFRP antennas [10, 11] have been reported for dual-band and broadband operations. In these studies, both crossed-dipole and NFRP elements were designed to generate CP radiations, which are utilized for the dual-band and broadband operations. Moreover, as mentioned in [10], an interesting phenomenon is that the polarization of the antenna can be changed by a physically adjusting the NFRP element. However, this phenomenon has not been rigorously pursued.

This paper investigates polarizations of a single-feed crossed-dipole antenna loaded with different NFRP elements. For the compact physical size, each arm of the crossed-dipole and NFRP elements contains a meander line with an arrowhead-shaped ending. The primary radiating elements are backed by a metallic reflector in order to improve the gain and achieve a broadside radiation pattern. It is

Received 23 September 2018, Accepted 26 October 2018, Scheduled 6 November 2018

* Corresponding author: Son Xuat Ta (xuat.tason@hust.edu.vn).

The author is with the School of Electronics and Telecommunications, Hanoi University of Science and Technology, Ha Noi, Viet Nam.

shown that the polarization of the antenna can be changed from right-hand CP (RHCP) — linearly polarized (LP) — left-hand CP (LHCP) radiations by adjusting the ending size of the individual NFRP arms. For verification, the RHCP and LHCP antennas have been realized and measured. Both designs yield a compact size, broad impedance matching bandwidth, and good broadside CP radiation (highly symmetric radiation pattern, high front-to-back ratio, and high RE). The results show big potential for designing compact polarization-reconfigurable antennas based on the crossed-dipole NFRP antenna, which is suitable for the use in several wireless communication systems, such as radio frequency identification (RFID), global navigation satellite system (GNSS), and wireless local area network (WLAN).

2. UNIDIRECTIONAL CROSSED-DIPOLE NFRP ANTENNA

Figure 1 shows the geometry of a crossed dipole antenna loaded with a NFRP element. The antenna was placed above a 150 mm × 150 mm ground plane at a distance of H_a. Its primary radiating elements are the same as those of the design presented in [10], which were printed on two substrates made of Rogers RT/duroid 5880 material ($\varepsilon_r = 2.2$ and $\tan\delta = 0.0009$) with thickness $h_{s1} = h_{s2} = 0.508$ mm. The substrates were stacked together with no air gap. The crossed dipole was printed on both sides of substrate 1, whereas the NFRP element was printed on the top side of substrate 2. The crossed dipole was incorporated with a pair of vacant-quarter printed rings to produce CP radiation and to match to the 50-Ω coaxial line without any matching network. For the compact size, meander-lines with an arrowhead-shaped trace at the end were employed in both crossed dipole and NFRP elements. The crossed dipole and NFRP elements were designed to produce desired CP radiations at different

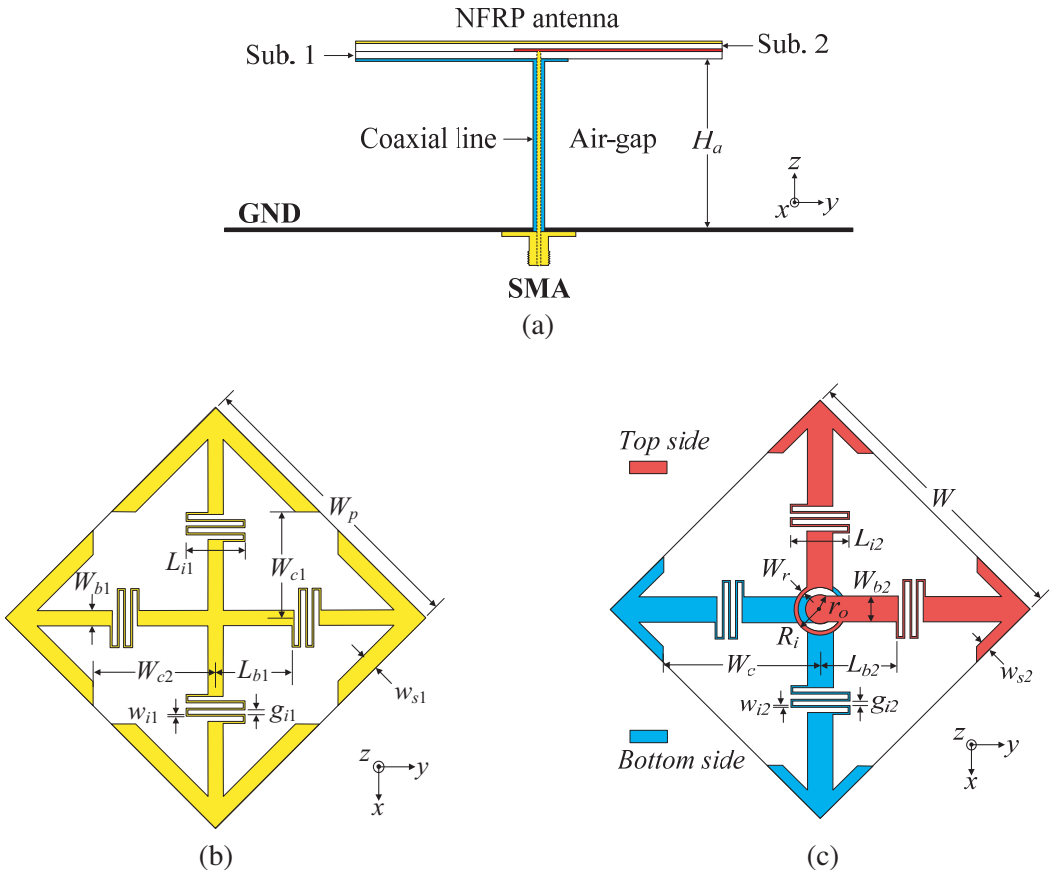

Figure 1. Geometry of the proposed antenna: (a) cross sectional view, (b) top view of NFRP element, and (c) top view of crossed-dipole element.

frequency bands, which were properly combined for a broadband CP radiation near 1.56 GHz. The antenna was characterized by using the ANSYS High-Frequency Structure Simulator (HFSS). Referring to Fig. 1, its optimized design parameters are: $H_a = 40$, $W_p = 35$, $W_{b1} = 1.8$, $W_{c1} = 13$, $W_{c2} = 15$, $L_{b1} = 7.6$, $w_{i1} = 0.2$, $g_{i1} = 0.6$, $L_{i1} = 7$, $w_{s1} = 2$, $W = 35$, $R_b = 3$, $W_r = 0.3$, $r_o = 1.3$, $W_{b2} = 2.6$, $W_c = 18.5$, $L_{b1} = 9.2$, $w_{i1} = 0.2$, $g_{i1} = 0.6$, $L_{i1} = 7$, and $w_{s2} = 1.3$ (unit in mm).

With the given parameters, the crossed-dipole NFRP antenna has a proper coupling between its elements; i.e., the horizontal dipole of the crossed-dipole element, which was the shorter dipole, was directly coupled with the smaller-ending arms of the NFRP element, whereas the vertical dipole, which was longer because of the addition of the ring, was directly coupled with the larger-ending arms of the NFRP element. The coupling produced a good impedance matching and good RHCP radiation at the

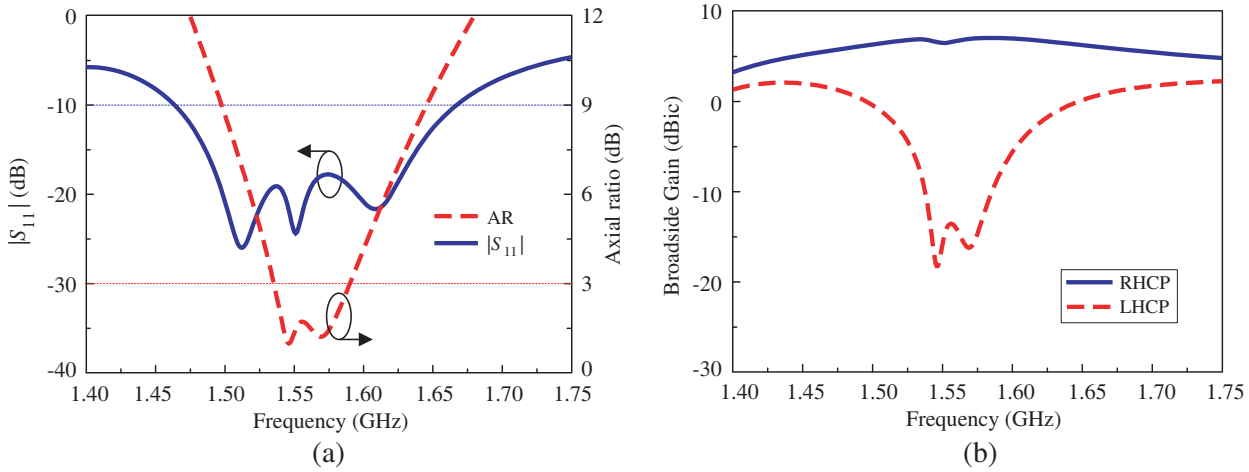

Figure 2. Simulated performances of the crossed dipole loaded with NFRP element on PEC reflector; (a) $|S_{11}|$ and AR values; (b) broadside RHCP and LHCP gains.

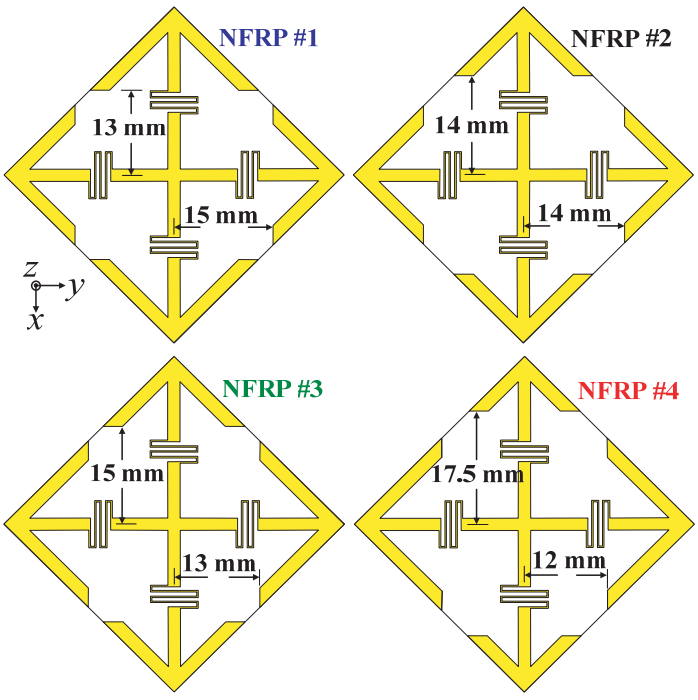

Figure 3. Top-view of the different NFRP elements.

broadside. This is confirmed in Fig. 2, which shows the simulated $|S_{11}|$, AR, and gain values of the antenna. As shown in Fig. 2(a), the crossed-dipole antenna loaded with the NFRP element yielded a bandwidth of 1.466–1.674 GHz (208 MHz) for $|S_{11}| < -10$-dB with three resonances at 1.514 GHz, 1.562 GHz, and 1.621 GHz. While it yielded a 3-dB AR bandwidths of 1.550–1.598 GHz (48 MHz) with two minimum points at 1.565 GHz (AR = 1.3 dB) and 1.576 GHz (AR = 1.56 dB). In free space, the crossed-dipole NFRP antenna radiated a bi-directional electromagnetic wave with a gain of < 2.0 dBic at both frequencies [10]. Due to the presence of the metallic reflector, the antenna yielded a good broadside RHCP radiation with a gain of > 6.6 dBic across the 3-dB AR bandwidth [Fig. 2(b)]. In addition, the HFSS indicated that the antenna had a RE of $> 77\%$.

3. POLARIZATION OF ANTENNA WITH DIFFERENT NFRP ELEMENTS

By physically adjusting the structure of the parasitic element, the polarization of the crossed-dipole NFRP antenna can be changed [10]. In order to investigate this phenomenon, a parametric study for different structures of the parasitic element (Fig. 3) was carried out. The NFRP #1 was the same as that given in Fig. 1(b), whereas other NFRP elements have the same design parameters as the NFRP #1 case except the arrowhead ends of the individual arms; i.e., from the NFRP #1 element to NFRP #4 element, the endings of the vertical arms was reduced, whereas those of the horizontal arms were increased.

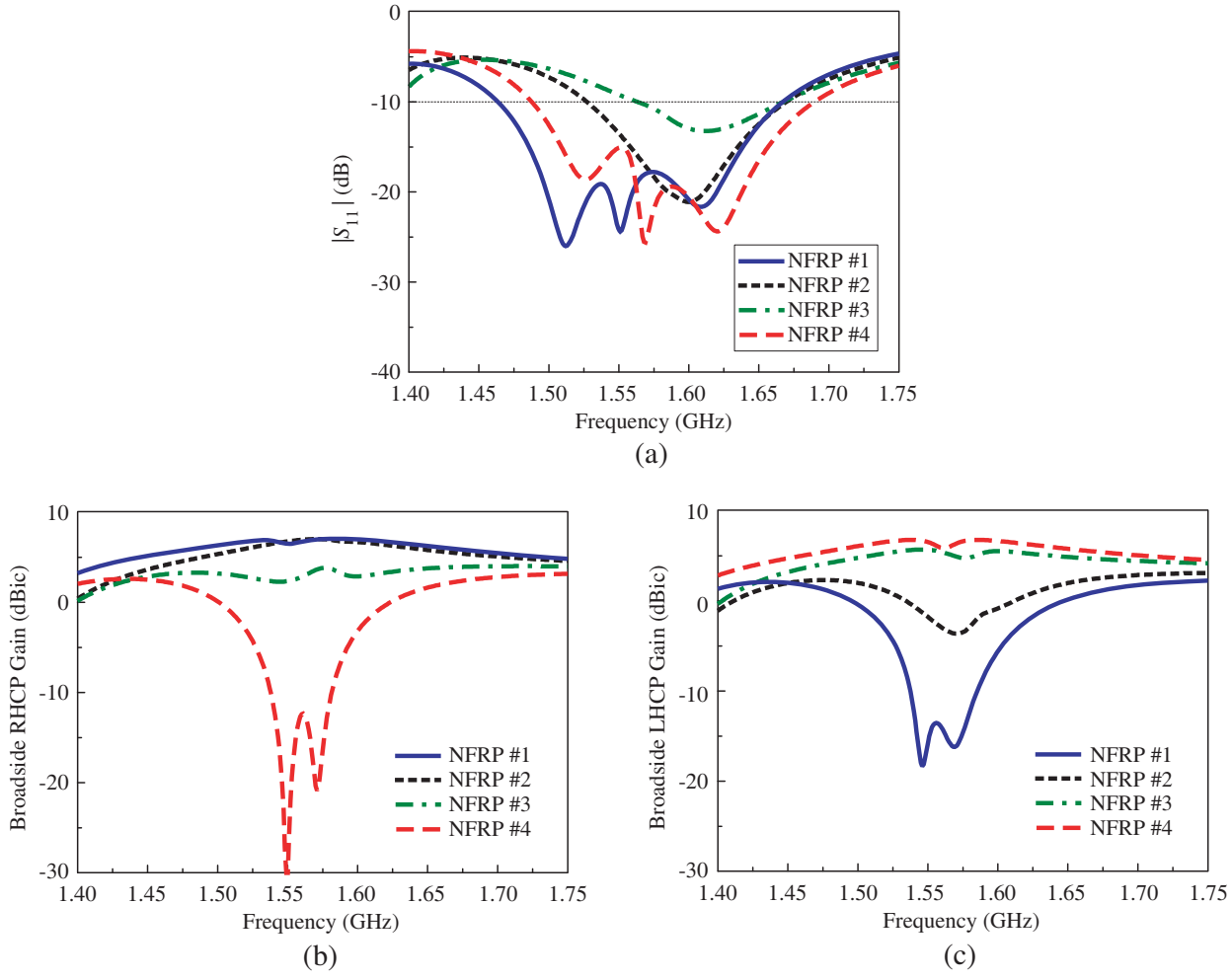

Figure 4. Simulated (a) $|S_{11}|$ values, (b) broadside RHCP, and (c) broadside LHCP gains of the crossed dipole antenna loaded with different NFRP elements.

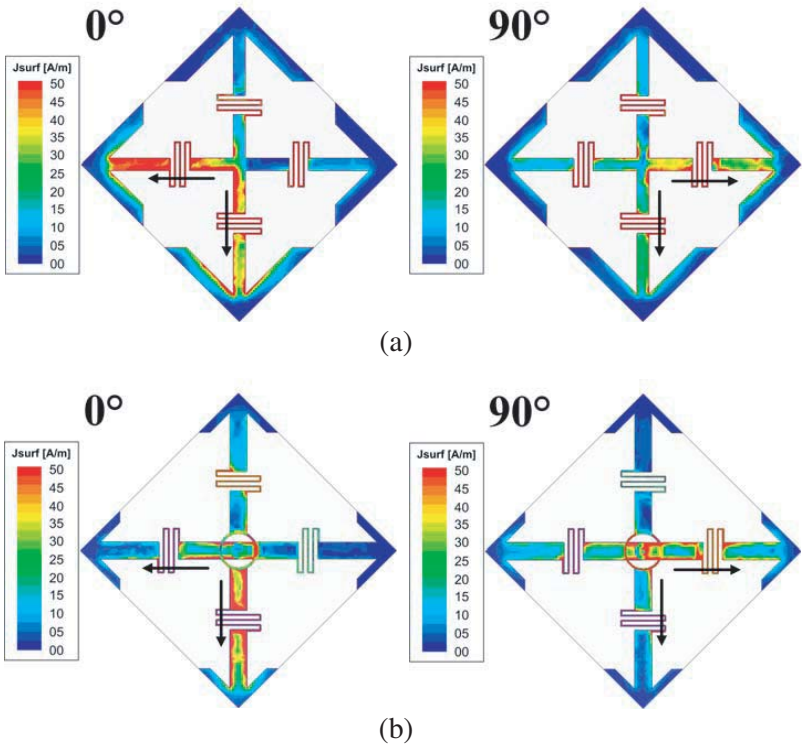

Figure 5. Current distribution at 1.56 GHz on (a) NFRP and (b) crossed-dipole elements of the NFRP#1 configuration at 0° and 90° phase angles.

Figure 4 shows the simulated $|S_{11}|$ and broadside gain values of the crossed-dipole antenna loaded with different NFRP elements illustrated in Fig. 3. As mentioned above, due to the proper coupling between its driven and parasitic elements, the NFRP #1 antenna yielded a good impedance matching and a good broadside RHCP radiation. For the NFRP #2 configuration, the impedance matching bandwidth degraded [Fig. 4(a)], while the RHCP gain reduced slightly [Fig. 4(b)], but the LHCP gain increased significantly [Fig. 4(c)] as compared to the NFRP #1 case. For the NFRP #3 case, the antenna yielded a similar value for RHCP and LHCP gains, and consequently, the antenna is nearly LP. Further reducing the endings of the vertical arms and increasing those of the horizontal arms, the antenna yielded a good impedance matching and a good LHCP radiation. From the HFSS predictions, the crossed-dipole antenna loaded with NFRP #4 element yielded $|S_{11}| < -10$ dB bandwidth of 1.485–1.680 GHz (195 MHz), 3-dB AR bandwidths of 1.530–1.585 GHz (55 MHz), gain of > 6.0 dBic, and RE of $> 67\%$. Similar to the case with NFRP #1, the antenna with NFRP #4 had three resonances at 1.520 GHz, 1.575 GHz, and 1.610 GHz in its $|S_{11}|$ profile and two CP frequency bands centered at 1.545 GHz and 1.575 GHz.

For better understanding the changes of polarization, the current distributions on the parasitic and crossed-dipole elements of the NFRP #1 and NFRP #4 cases were computed for different phase angles. The current distributions were calculated at 1.56 GHz and are given in Figs. 5 and 6. For both configurations, the current distributions were not very symmetric on their elements. This behavior is because the crossed dipoles are placed on different sides of the substrate 1, which causes the different near-field couplings between the parasitic and the dipole arms [10]. As shown in Fig. 5, the currents on both NFRP #1 and crossed-dipole elements rotated counterclockwise. This confirmed that the NFRP#1 antenna radiates RHCP. As shown in Fig. 6, the currents on both NFRP#4 and crossed-dipole elements rotated clockwise. Thus, the antenna is LHCP.

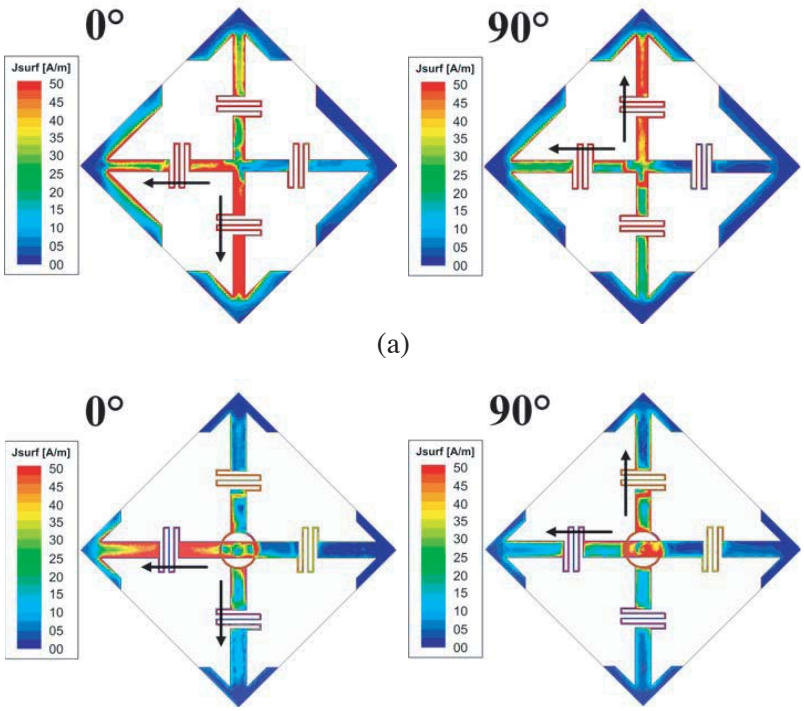

Figure 6. Current distribution at 1.56 GHz on (a) NFRP and (b) crossed-dipole elements of the NFRP#4 configuration at 0° and 90° phase angles.

4. MEASUREMENTS

For verification, the crossed-dipole antennas loaded with NFRP #1 and #4 elements were fabricated and measured. The crossed dipole and NFRP elements were implemented on Rogers RT/Duroid^{TM} 5880 substrates with a copper thickness of 17 µm via a standard wet-etching technology. To simplify the fabrication, thin tapes were used to fasten the elements of the prototypes.

Figure 7(a) shows a fabricated sample of the NFRP #1 configuration including a 150 mm × 150 mm metallic reflector. Its simulated and measured results are given in Figs. 7(b), (c). It is observed that the measurements agreed rather closely with the HFSS predictions. As shown in Fig. 7(b), the measurements resulted in a $|S_{11}| < -10$ dB bandwidth of 1.454–1.668 GHz (214 MHz) and a 3-dB AR bandwidth of 1.525–1.585 GHz (60 MHz), whereas the simulated $|S_{11}| < -10$ dB and 3-dB AR bandwidths are 1.464–1.667 GHz (203 MHz) and 1.535–1.590 GHz (55 MHz), respectively. As shown in Fig. 7(c), the NFRP#1 antenna yielded a good broadside RHCP radiation with symmetric profile and high front-to-back (F-B) ratio. At 1.56 GHz, the measurements resulted in a gain of 6.5 dBic, F-B ratio of 14.0 dB, and half-power beamwidth (HPBW) of 62° and 59° in the x-z and y-z planes, respectively. Additionally, the measurements resulted in a RE of greater than 70% compared with the simulated value of greater than 77% across the 3-dB AR bandwidth.

A fabricated sample of the NFRP #4 antenna is illustrated in Fig. 8(a), and its simulated and measured results are shown in Figs. 8(b), (c). Again, there was a good agreement between the measurements and the HFSS simulations. As shown in Fig. 8(b), the measured $|S_{11}| < -10$ dB bandwidth was 1.475–1.702 GHz (227 MHz) compared with the simulated value of 1.488–1.689 GHz (201 MHz), while its measured 3-dB AR bandwidth was 1.535–1.580 GHz (45 MHz) related to the simulated one of 1.536–1.584 GHz (48 MHz). As shown in Fig. 8(c), the antenna with NFRP #4 resulted in a good broadside LHCP radiation with symmetric profile and high F-B ratio. At 1.56 GHz, the antenna yielded a gain of 6.4 dBic, F-B ratio of 15.2 dB, and HPBWs of 77° and 76° in the x-z and

y-z planes, respectively. Additionally, the measurements yielded an RE of $> 65\%$, while the simulated value was $> 67\%$ across the 3-dB AR bandwidth.

Table 1 shows a performance comparison between the proposed antenna and the previous single-feed CP NFRP antennas. Although the proposed antennas are not electrically small ($ka = 1.57$ at 1.56 GHz) due to the presence of the ground plane, their primary radiating elements are still compact ($ka = 0.81$ at 1.56 GHz). In the proposed designs, the ground plane acts as a reflector for the broadside

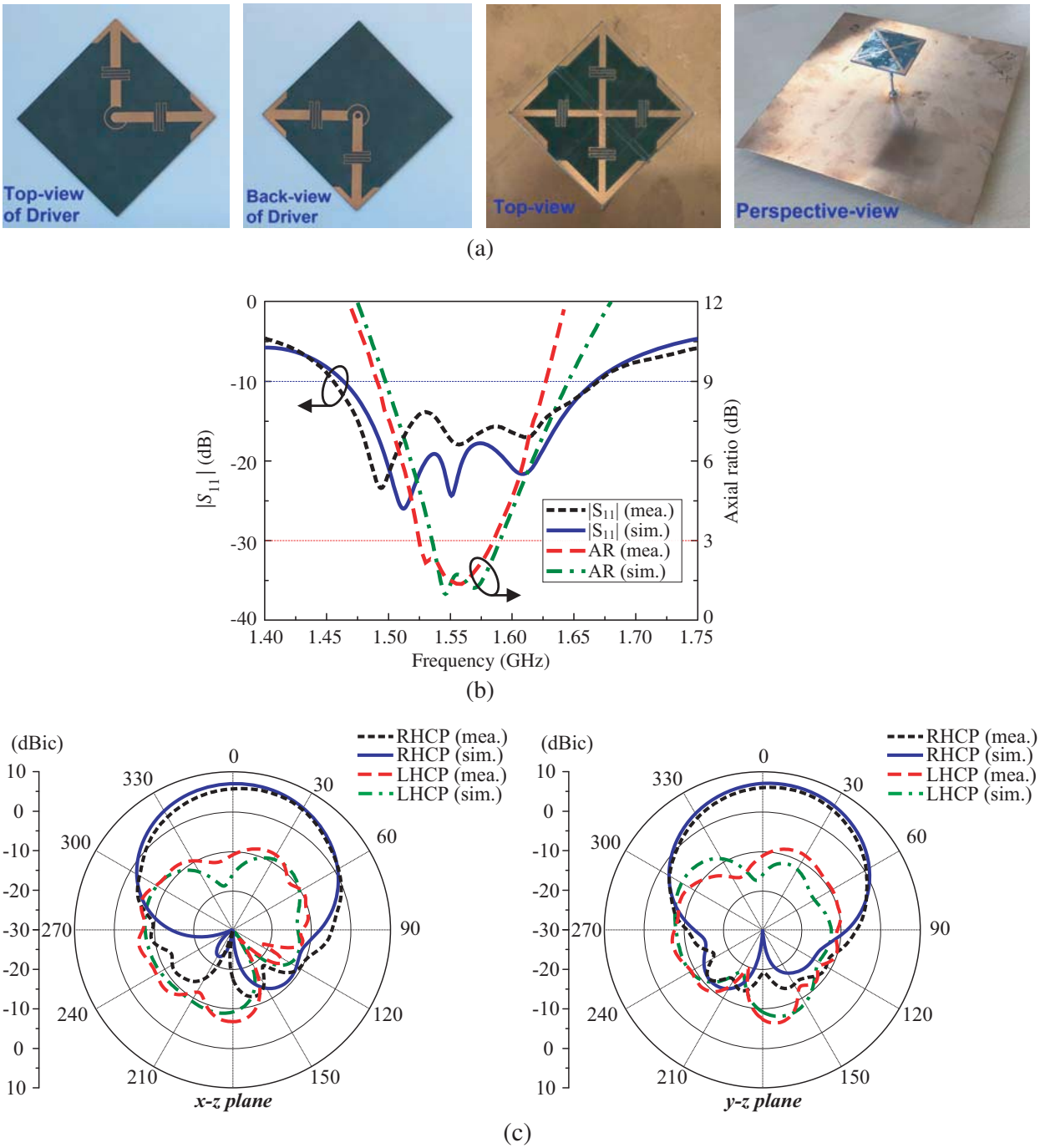

Figure 7. (a) Fabricated sample of the RHCP design. Simulations and measurements: (b) $|S_{11}|$ and AR values, and (c) 1.56 GHz radiation pattern.

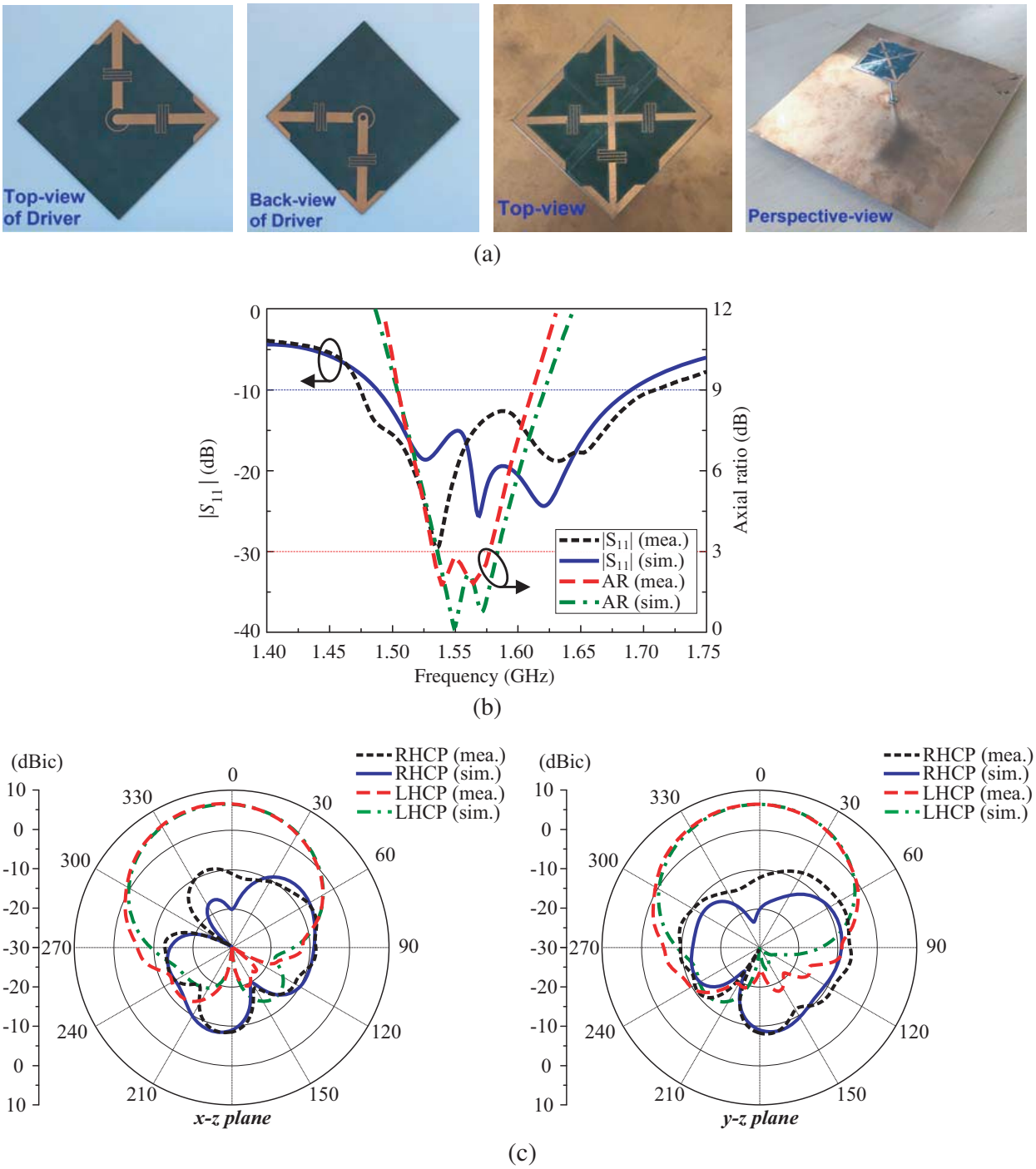

Figure 8. (a) Fabricated sample of the LHCP design. Simulation and measurements: (b) $|S_{11}|$ and AR values, and (c) 1.56 GHz radiation pattern.

radiation pattern, whereas the antenna bandwidths are mainly determined by the primary radiating elements. Compared to the priors [5–8], the proposed antennas have simpler configurations and larger bandwidths in terms of impedance matching and 3-dB AR.

Table 1. Performance comparison between the proposed designs and the previous single-feed CP NFRP antennas.

Antenna structures	Antenna size (ka)	Configuration	$\|S_{11}\| < -10$ dB BW (%)	AR < 3-dB BW (%)	RE (%)	Gain (dBic)
RHCP	1.57	On GND	13.7	3.86	70.0	6.5
LHCP	1.57	On GND	14.29	2.89	65	6.4
Ref. [5]	0.495	On GND	1.955	0.44	96.9	6.28
Ref. [6]	0.5 (L)	On GND	0.86 (L), 1.54 (U)	0.35 (L), 0.34 (U)	71.1 (L), 79.2 (U)	5.36 (L), 6.20 (U)
Ref. [7]	0.30	In free space	4.5	0.886	73.4	1.38
Ref. [8]	0.99	On AMC	3.1	0.736	79.6	4.25

L: lower frequency band, U: upper frequency band, AMC: artificial magnetic conductor, a is the radius of the smallest sphere enclosing the entire antenna and $k = 2\pi/\lambda_0$, λ_0 being the free-space wavelength corresponding to its resonance frequency: f_0.

5. CONCLUSION

Single-feed crossed-dipole antennas loaded with different NFRP elements have been investigated. The antennas are placed above metallic reflectors for a broadside radiation pattern. By adjusting the ending sizes of the individual NFRP arms, the polarization of the antenna can be RHCP-LP-LHCP. For verification, the antennas with RHCP and LHCP performances are fabricated and measured. Comparisons between the simulations and measurements demonstrate that both antennas have broadband characteristics and a good broadside CP radiation with highly symmetric radiation profile, high F-B ratio, and high RE. With these features, the proposed antennas can be widely applied to a variety of wireless systems operating near 1.56 GHz. Also, this study demonstrates the big potential to implement compact polarization-reconfigurable antennas based on the crossed-dipole NFRP antenna, which could be widely used in several wireless communication systems, such RFID, GNSS, as well as WLAN.

ACKNOWLEDGMENT

This research is funded by Vietnam National Foundation for Science and Technology Development (NAFOSTED) under grant number 102.04-2016.02.

REFERENCES

1. Ziolkowski, R. W., P. Jin, and C. Lin, "Metamaterial-inspired engineering of antennas," *IEEE Proc.*, Vol. 99, No. 10, 1720–1731, Oct. 2011.
2. Dong, Y. and T. Itoh, "Metamaterial-based antennas," *IEEE Proc.*, Vol. 100, No. 7, 2271–2285, Jul. 2012.
3. Erentok, A. and R. W. Ziolkowski, "Metamaterial-inspired efficient electrically-small antennas," *IEEE Trans. Antennas Propag.*, Vol. 56, No. 3, 691–707, Mar. 2008.
4. Jin, P. and R. W. Ziolkowski, "Multiband extensions of the electrically small metamaterial-engineered Z antenna," *IET Microw. Antennas Propag.*, Vol. 4, 1016–1025, Aug. 2010.
5. Lin, C., P. Jin, and R. W. Ziolkowski, "Multi-functional, magnetically-coupled, electrically small, near-field resonant parasitic wire antennas," *IEEE Trans. Antennas Propag.*, Vol. 59, No. 3, 714–724, Mar. 2011.
6. Jin, P. and R. W. Ziolkowski, "Multi-frequency, linear and circular polarized, metamaterial-inspired, near-field resonant parasitic antennas," *IEEE Trans. Antennas Propag.*, Vol. 59, No. 5, 1446–1459, May 2011.

7. Jin, P., C. Lin, and R. W. Ziolkowski, "Multifunctional, electrically small, planar near-field resonant parasitic antennas," *IEEE Antennas Wireless Propag. Lett.*, Vol. 11, 200–204, 2012.
8. Jin, P. and R. W. Ziolkowski, "High directivity, electrically small, low-profile, near-field resonant parasitic antennas," *IEEE Antennas Wireless Propag. Lett.*, Vol. 11, 305–309, 2012.
9. Tang, M., B. Zhou, and R. W. Ziolkowski, "Low-profile, electrically small, Huygens source antenna with pattern-configurability that covers the entire azimuthal plane," *IEEE Trans. Antennas Propag.*, Vol. 65, No. 3, 1063–1072, Mar. 2017.
10. Ta, S. X., K. Lee, I. Park, and R. W. Ziolkowski, "Compact crossed-dipole antenna loaded with near-field resonant parasitic element," *IEEE Trans. Antennas Propag.*, Vol. 65, No. 2, 482–488, Feb. 2017.
11. Ta, S. X., I. Park, and R. W. Ziolkowski, "Broadband circularly polarized NFRP antenna using crossed dipole driver," *11th European Conference on Antennas and Propagation (EuCAP)*, 1972–1975, Paris, France, Mar. 2017.